Translational Oncology 13 (2020) 100853

Contents lists available at ScienceDirect

Translational Oncology

journal homepage: www.elsevier.com/locate/tranon

Oncogenic fusion protein FGFR2-PPHLN1: Requirements for biological activation, and efficacy of inhibitors

Fangda Li [a], April N. Meyer [a], Malalage N. Peiris [a], Katelyn N. Nelson [a], Daniel J. Donoghue [a,b,*]

[a] Department of Chemistry and Biochemistry, University of California San Diego, La Jolla, CA 92093-0367, USA
[b] UCSD Moores Cancer Center and Department of Chemistry and Biochemistry, University of California San Diego, La Jolla, CA 92093-0367, USA

ARTICLE INFO

Article history:
Received 2 May 2020
Received in revised form 24 July 2020
Accepted 9 August 2020
Available online xxxx

ABSTRACT

Aim of study: Chromosomal translocations such as t(10;12)(q26,q12) are associated with intrahepatic cholangiocarcinoma, a universally fatal category of liver cancer. This translocation creates the oncogenic fusion protein of Fibroblast Growth Factor Receptor 2 joined to Periphilin 1. The aims of this study were to identify significant features required for biological activation, analyze the activation of downstream signaling pathways, and examine the efficacy of the TKIs BGJ398 and TAS-120, and of the MEK inhibitor Trametinib.

Methods: These studies examined FGFR2-PPHLN1 proteins containing a kinase-dead, kinase-activated, or WT kinase domain in comparison with analogous FGFR2 proteins. Biological activity was assayed using soft agar colony formation in epithelial RIE-1 cells and focus assays in NIH3T3 cells. The MAPK/ERK, JAK/STAT3 and PI3K/AKT signaling pathways were examined for activation. Membrane association was analyzed by indirect immunofluorescence comparing proteins altered by deletion of the signal peptide, or by addition of a myristylation signal.

Results: Biological activity of FGFR2-PPHLN1 required an active FGFR2-derived tyrosine kinase domain, and a dimerization domain contributed by PPHLN1. Strong activation of canonical MAPK/ERK, JAK/STAT3 and PI3K/AKT signaling pathways was observed. The efficacy of the tyrosine kinase inhibitors BGJ398 and TAS-120 was examined individually and combinatorially with the MEK inhibitor Trametinib; heterogeneous responses were observed in a mutation-specific manner. A requirement for membrane localization of the fusion protein was also demonstrated.

Concluding statement: Our study collectively demonstrates the potent transforming potential of FGFR2-PPHLN1 in driving cellular proliferation. We discuss the importance of sequencing-based, mutation-specific personalized therapeutics in treating FGFR2 fusion-positive intrahepatic cholangiocarcinoma.

Introduction

Intrahepatic cholangiocarcinoma (ICC) is an often-fatal liver cancer which arises in the biliary ducts [1,2]. The genesis of ICC involves various genetic alterations, such as activating mutations in receptor tyrosine kinases (RTKs), and oncogenic fusion proteins involving RTKs as partner genes [1,3]. To date, all of the oncogenic fusion proteins identified in ICC involve the identical portion of Fibroblast Growth Factor Receptor 2 (FGFR2) (exons 1–19) fused with diverse dimerization partners [1,4]. The translocation t(10;12)(q26,q12), fusing FGFR2 with Periphilin 1 (PPHLN1), accounts for approximately 16% of ICC [1,5].

FGFR2 is a transmembrane RTK that belongs to the four-membered FGFR family, FGFR1–4. Upon binding of Fibroblast Growth Factors (FGFs), FGFRs undergo receptor dimerization leading to trans-autophosphorylation on tyrosine residues of the receptor and adaptor proteins, resulting in downstream signaling [6]. Mutations in FGFR2 have a long history in human developmental syndromes such as Crouzon, Pfeiffer, and Apert syndromes, as well as carcinogenesis [7].

The fusion partner, Periphilin-1 (PPHLN1), localizes in nuclear granules in undifferentiated keratinocytes, but colocalizes with periplakin at the cell periphery and at cell-cell junctions following keratinocyte differentiation [8], becoming incorporated into the cornified cell envelope. Its C-terminus contains a coiled-coil domain with 7 heptad repeats, of which the C-terminal 25 residues are sufficient for self-dimerization [8]. Thus, the PPHLN1 moiety drives dimerization of the FGFR2-PPHLN1 fusion protein, potentially leading to ligand-independent hyperactivation of FGFR2 kinase domain.

Several pan-FGFR tyrosine kinase inhibitors (TKIs) have been studied clinically for treating FGFR2-fusion specific ICC patients, including BGJ398, Ponatinib, and PD173074. Of these, BGJ398 has shown promising

* Corresponding author at: Department of Chemistry and Biochemistry, University of California San Diego, La Jolla, CA 92093-0367, USA.
E-mail address: ddonoghue@ucsd.edu. (D.J. Donoghue).

http://dx.doi.org/10.1016/j.tranon.2020.100853

anti-tumor activity with manageable toxicity at early stages of treatment [9–11]. However, a subset of patients treated with BGJ398 and other TKIs develops mutations, including N549H, E565A and K641R in FGFR2, that confer resistance [6,11–13]. Normally, N549, E565 and K641 form a triad coordinated by hydrogen bonding which restrains the FGFR2 kinase. Mutations of these residues stabilize the kinase domain in an activated conformation [13]. TAS-120, a third-generation irreversible pan-FGFR inhibitor, binds covalently to a highly conserved cysteine in the ATP pocket of FGFR, emerging as a promising candidate against FGFR2 fusion-positive ICC [14].

Here, we examined the requirements of FGFR2-PPHLN1 to drive cellular proliferation, including signaling mechanisms, subcellular localization, and the effects of the activating mutation N550K. Furthermore, we examined the effects of several inhibitors on the activity of FGFR2-PPHLN1.

Materials and methods

FGFR2-PPHLN1 constructs

The myc-tagged PPHLN1 gene (OriGene Technologies, Inc., clone RC216262) was subcloned into pcDNA3. FGFR2 constructs have been previously described in prior publications [15,16]. FGFR2 kinase active N550K/N549K and kinase dead mutations K518R/K517R for IIIb and IIIc isoforms, respectively, were made by Quickchange site-directed mutagenesis (Agilent). For FGFR2-IIIb-PPHLN1 constructs, the codon for residue E768 of FGFR2-IIIb (Uniprot P21802-3, Isoform 3, KGFR) was joined directly to the codon for residue D32 of PPHLN1 (Uniprot QNEY8-2, Isoform 2). For FGFR2-IIIc-PPHLN1 constructs, the codon for residue E767 of FGFR2-IIIc (Uniprot P21802-1, Isoform 1, BEK) was joined directly to the codon for residue D32 of PPHLN1 (Uniprot QNEY8-2, Isoform 2).

For derivation of plasma membrane-localized proteins, a myristylation signal from c-Src was utilized as described [17,18]. To create ΔSS-FGFR2-IIIc-PPHLN1, residues 2–26 were deleted as previously described [19]. The pcDNA3 expression vector was used for transient transfections in HEK293T and NIH3T3cells, and the neomycin-selectable retroviral vector pLXSN [20] was used for biological assays in NIH3T3 and RIE-1 cells. The accuracy of all DNA constructs was fully validated by sequencing.

Cell culture, immunoblotting and immunofluorescence

HEK293T cells were maintained in DMEM plus 10% FBS and 1% penicillin/streptomycin in 10% CO_2 at 37 °C. HEK293T cells were plated at a density of 1×10^6 cells/100-mm plate and transfected with plasmid DNA using calcium phosphate transfection in 3% CO_2 as described previously [21]. Twenty to 24 h after transfection, media were changed to DMEM with 0% FBS. Cells were starved for 20 h before collecting and lysis [22]. HEK293T cells were collected, washed once in PBS, and lysed in RIPA buffer [50 mM Tris-HCl (pH 8.0), 150 mM NaCl, 1% TritionX-100, 0.5% sodium deoxycholate, 0.1% SDS, 50 mM NaF, 1 mM sodium orthovanadate, 1 mM PMSF, and 10 mg/ml aprotinin]. Lowry assay was used to measure total protein concentration. Samples were separated by 12.5% SDS-PAGE and transferred to Immobilon-P membranes (Millipore). Immunoblotting was performed as described previously [23].

NIH3T3 cells were maintained in 10% calf serum and 1% penicillin/streptomycin in 10% CO_2 at 37 °C. Focus assays were performed as described previously [24]. Briefly, cells plated at a density of 4×10^5 cells/60-mm plates in DMEM with 10% calf serum 24 h before transfection. Cells were transfected using Lipofectamine 2000 Reagent with 10 μg plasmid DNA. Approximately 48 h after transfection cells were split 1:12 onto duplicate 100-mm plates with 2.5% calf serum. Foci were scored at 14 days, fixed in methanol, and stained using Geimsa stain. Efficiency of transfection was determined by Geneticin (G418, 0.5 mg/ml)-resistant colonies plated on duplicate plates at a dilution of 1:240.

RIE-1 cells were maintained in 5% calf serum and 1% penicillin/streptomycin in 10% CO_2 at 37 °C. RIE-1 stable cell lines were generated by selecting Lipofectamine 2000 transfected cells with 0.5 mg/ml G418, with multiple cell lines for each clone. These cells were maintained and frozen in the presence of 0.5 mg/ml G418. For soft agar assays, 2.5×10^5 cells were seeded per 60 mm dish in medium containing 0.3% agarose over a base layer of 0.6% agarose. Media was layered on top and changed or supplemented twice weekly. These assays were conducted in triplicate, with 3 individual plates for each concentration.

For indirect immunofluorescence, NIH3T3 cells were transiently transfected by calcium phosphate, as described above. Cells were seeded at 2×10^5 cells in 60-mm plates containing glass coverslips (Neuvitro, Vancouver,WA, USA). Twenty four hours after transfection, media were changed to DMEM with 0% calf serum and starved for 18 h. Immunofluorescence staining was performed essentially as previously described [17]. Briefly, cells were fixed with 4% paraformaldehyde/PBS, permeabilized with 0.1% Triton X-100/PBS, blocked with 5% BSA/PBS and incubated with primary antibody, c-Myc (9E10). After washes, cells were treated with secondary antibody, Alexa Fluor 488 donkey anti-mouse. Nuclei were visualized with Hoechst 33342 (1 μg/ml). Coverslips were mounted with Prolong Gold anti-fade reagent (Invitrogen, Carlsbad, CA, USA). Cells were examined on a Leica SP8 inverted confocal microscope (UC San Diego Neuroscience Core Facility).

Antisera reagents were: Bek (H-80), Bek (C-8), c-Myc (9E10), and STAT3 (C-20), from Santa Cruz Biotechnology (Dallas, TX, USA); phospho-STAT3 (Tyr705; D3A7), p44/42 MAPK (ERK 1/2, 9102), phospho-p44/42 MAPK (Erk1/2) (Thr202/Tyr204) (D13.14.4E), phospho-FGFR (Tyr653/654, 3471), AKT (9272), and phospho-Akt (S473, D9E) from Cell Signaling (Danvers, MA, USA); FGFR2 N-terminal (ab75984) from Abcam (Burlingame, CA, USA); Alexa Fluor 488 donkey anti-mouse (A21202) from Invitrogen (Carlsbad, CA, USA); horseradish peroxidase (HRP) anti-mouse, HRP anti-rabbit, and Enhanced Chemiluminence (ECL and Prime-ECL) reagents were from GE Healthcare (Little Chalfont, UK). Immunoblots presented in this work are representative of at least three replications using different lysates from cells.

Other reagents and sources were: Geneticin (G418), Gibco (Waltham, MA, USA); Lipofectamine 2000, Invitrogen (Carlsbad, CA, USA); PNGaseF (P0704S), NEB (Ipswich, MA, USA); Trametinib (GSK 1120212) (S2673) and BGJ398 (NVP-BGJ398), Selleckchem (Houston, TX, USA), and TAS-120 (C-1520), Chemgood (Glen Allen, VA, USA).

Inhibitor treatments

Transfected HEK293T cells expressing either FGFR2-IIIc-PPHLN1 or FGFR2-IIIc-N549K-PPHLN1 were treated with inhibitors singly or in combination during the last 3 h of starvation at 10% CO_2 in 0% FBS in DMEM medium. HEK293T cells were collected, washed once in PBS, and lysed in RIPA, as described above. RIE-1 cells stably expressing FGFR2-IIIb-PPHLN1 or FGFR2-IIIb-N550K-PPHLN1, described above, were plated in soft agar assays in the presence of Trametinib, BGJ398, or TAS-120 or in combination for three weeks. These assays were conducted in triplicate, with 3 individual plates for each concentration. Colonies were stained with crystal violet and quantitated using ImageJ.

Results

Soft agar colony formation of FGFR2-IIIb-PPHLN1

Clones shown in Fig. 1A were assayed by soft agar colony formation in RIE-1 cells for IIIb mutants, or by focus formation assay in NIH3T3 cells for IIIc mutants. These constructs fuse exon 19 of FGFR2-IIIb to exon 4 of PPHLN1, recapitulating the most common translocation breakpoint for t(10;12)(q26,q12) [5]. We included kinase-activated N550K/N549K mutant, corresponding to the FGFR3 N540K mutation first identified as causing the human skeletal dysplasia hypochondroplasia [25]. As described above, N550/N549 participates in a molecular brake for the FGFR2 kinase activity. This mutation occurs in FGFR2-fusion proteins harbored by ICC patients, conferring resistance to BGJ398 [12]. These assays included the kinase-dead mutation K518R/K517R in the ATP binding site [26]. The

IIIb isoform is predominantly expressed in epithelial cells; therefore, most carcinomas, including cholangiocarcinomas, which are driven by activated FGFR2 will exhibit the IIIb isoform. In contrast, the IIIc isoform is predominantly expressed in mesenchymal and hematopoietic cancers; these cancers will typically express the IIIc isoform. Identical mutations may arise in FGFRs in both types of cancers, although the actual residue number will differ due to slightly different lengths of alternatively spliced exons. Throughout the experiments which follow, we have used both IIIb and IIIc isoforms, and we have used both epithelial cell lines as well as fibroblast cell lines; throughout, the specific isoform, the mutation number, and the cell line used for different assays have been consistently identified. While this may cause some confusion, we believe it appropriate to emphasize this distinction given that the properties of FGFR2 and FGFR2-PPHLN1 fusions differ in important respects depending upon the isoform and the cell type in which they are expressed.

As epithelial cells, RIE-1 cells express FGFs of epithelial origin, incapable of activating the IIIb isoform of FGFR2 [27–29]. When RIE-1 cells were assayed for soft agar colony formation, no colonies were observed for any FGFR2-IIIb clones: wild-type, kinase-activated, or kinase-dead (Fig. 1B, a–c). Significant colony formation was observed for FGFR2-IIIb-PPHLN1 and for the kinase-activated mutant (Fig. 1B, d–e). No colony formation was observed for the kinase-dead mutant (Fig. 1B, f). The loss of activity exhibited by the kinase-dead mutant demonstrates a requirement for a functional tyrosine kinase domain within the FGFR2-derived moiety. These results were quantitated in Fig. 1C.

Similar FGFR2 and FGFR2-PPHLN1 clones were created in the background of FGFR2-IIIc. These were examined for focus formation using NIH3T3 cells, mesenchymal cells which expresses FGFs incapable of activating the IIIc isoform of FGFR2 [9,24]. Again, only FGFR2-IIIc-PPHLN1 and the kinase-activated fusion protein FGFR2-IIIc-N549K-PPHLN1 yielded robust focus formation as shown in Fig. 1D and quantitated in Fig. 1E.

Downstream signaling activation by FGFR2-PPHLN

FGFR2-IIIc and FGFR2-IIIc-PPHPLN1 proteins were expressed in HEK293T cells and lysates examined by immunoblotting. The FGFR2 activation status was examined using an antiserum that detects phosphorylated tyrosine residues within the FGFR2 activation loop. A dramatic increase

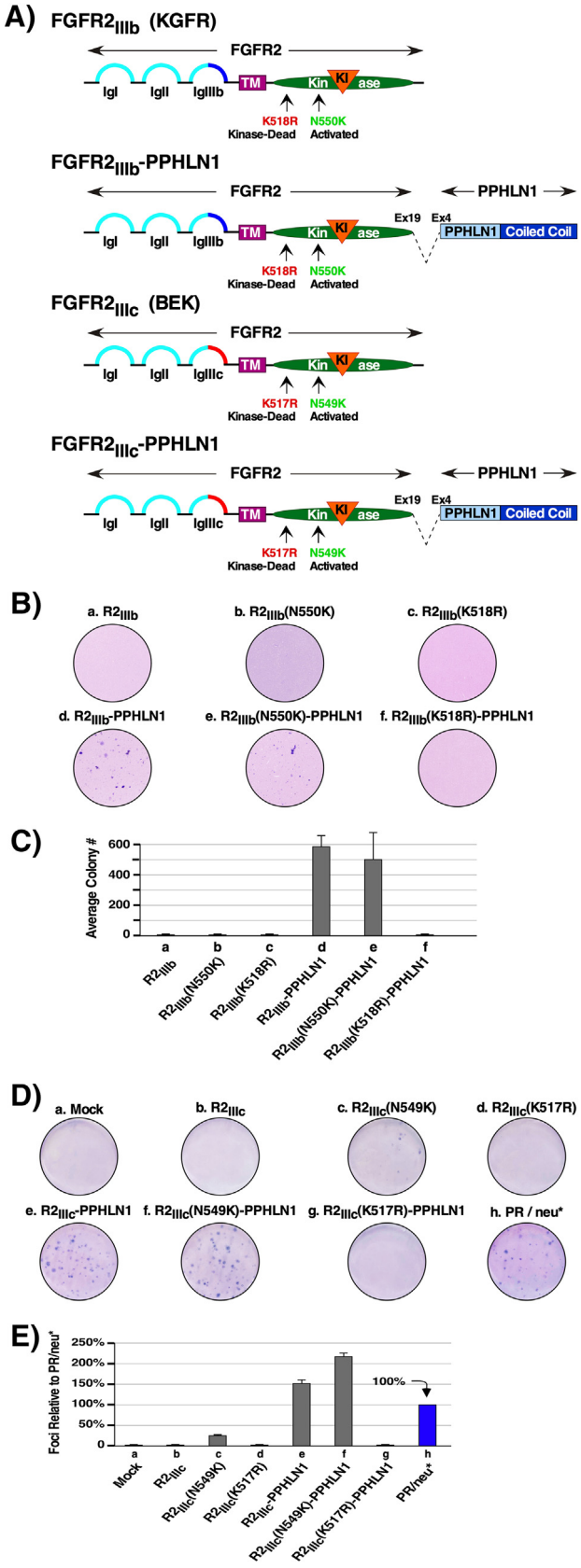

Fig. 1. Structure and biological assays of FGFR2-PPHLN1 constructs. (A) The top presents FGFR2-IIIb and FGFR2-IIIb-PPHLN1 with K518R kinase dead, and N550K kinase activating mutations, shown. FGFR2 contains an extracellular ligand binding domain with immunoglobulin-like domains (Ig), a transmembrane domain (TM), a split tyrosine kinase domain, and kinase insert domain (KI). FGFR2-IIIb-PPHLN1 contains FGFR2-IIIb through exon 19 at the N-terminus, fused to exon 4 of PPHLN1 at the C-terminus, which contains a coiled-coil domain. The alternatively spliced exon 8 of FGFR2, encoding the 3rd Ig-like domain, is shown in dark blue. This confers ligand specificity to FGFR2-IIIb for FGFs of mesenchymal origin; this receptor is specifically activated by FGFs of mesenchymal origin such as FGF3, FGF7, FGF10, or FGF22. Historically, FGFR2-IIIb has also been referred to as Keratinocyte Growth Factor Receptor (KGFR). The bottom presents FGFR2-IIIc and FGFR2-IIIc-PPHLN1 with K517R kinase dead, and N549K kinase activating mutations. The alternatively spliced exon 9 of FGFR2, encoding the 3rd Ig-like domain, is shown in red. This confers ligand specificity to FGFR2-IIIc; this receptor is specifically activated by FGFs of epithelial origin such as FGF1, FGF2, FGF4, FGF6, FGF9, FGF16, or FGF20. Note that exon 9 of IIIc encodes one residue less than exon 8 of IIIb, changing the numbering of all downstream residues. Historically, FGFR2-IIIc has also been known as BEK, referring to its initial discovery as a Bacteria-Expressed Kinase. (B) Soft agar colony formation by FGFR2-IIIb-PPHLN1 in RIE-1 cells. Representative plates from a soft agar colony formation assay are shown, with transfected constructs indicated. (C) Graph shows the average number of colonies ± SEM, using triplicate plates for each cell line. Plates stained with crystal violet. (D) Cell transformation of NIH3T3 cells by FGFR2-IIIc-PPHLN1. Representative plates from a focus assay are shown, with transfected constructs indicated. (E) The graph shows the number of foci scored, normalized for transfection efficiency and calculated as a percentage of transformation relative to PR/neu* ± SEM. Assays were performed a minimum of 3 times per each DNA construct. Plates were fixed and stained with Giemsa stain. (For interpretation of the references to colour in this figure legend, the reader is referred to the web version of this article.)

was observed in tyrosine phosphorylation for FGFR2-IIIc-PPHLN1 compared to FGFR2-IIIc (Fig. 2, 2nd panel, Lanes 2 & 5). The kinase activation observed by the fusion with PPHLN1 appears to be near-maximal; incorporation of the kinase-activating mutation into FGFR2-IIIc-N549K-PPHLN1 results in just a slight increase (Lanes 5–6). Incorporation of the kinase-dead mutation K517R, whether in FGFR2-IIIc-K517R or FGFR2-IIIc-K517R-PPHLN1, completely eliminates kinase activation (Lanes 4 & 7).

With regards to downstream signaling, significant activation of MAPK signaling (Fig. 2, 3rd panel) is observed in response to the strongly activated mutants: FGFR2-IIIc-N549K, FGFR2-IIIc-PPHPLN1, and FGFR2-IIIc-N549K-PPHLN1 (Lanes 3, 5, 6). Similar results are observed for activation STAT3, shown by phospho-STAT3 (5th panel, Lanes 3, 5, 6). Additionally, modest activation of Protein Kinase B (Akt) is observed for FGFR2-IIIc-PPHPLN1 and FGFR2-IIIc-N549K-PPHLN (7th panel, Lanes 5–6). No activation of any signaling pathway was observed in response to the kinase-dead proteins (3rd, 5th, and 7th panels, Lanes 4, 8). Thus, in the absence of FGF stimulation, activation of signaling pathways depends upon activation of the FGFR2 tyrosine kinase by fusion to PPHLN1, or by incorporation of the kinase-activating mutation. The coiled-coil domain of PPHLN1 confers constitutive activation to the kinase of the fusion protein, leading to hyperactivation of signaling.

Effect of Trametinib and TKIs on soft agar colony formation

RIE-1 cells stably expressing either FGFR2-IIIb-PPHLN1 or kinase-activated FGFR2-IIIb-N550K-PPHLN1 were examined by soft agar colony assay in the presence of one MEK inhibitor and two different TKIs (Fig. 3). We note that the experiments shown in Fig. 3A–E were conducted at different times with respect to each other; this produced some experimental variability which was difficult to eliminate completely in these experiments, but which did not alter the overall conclusions. The MEK inhibitor, Trametinib, blocked colony formation by FGFR2-IIIb-PPHLN1 and FGFR2-IIIb-N550K-PPHLN1 (Fig. 3A). The TKIs examined, BGJ398 and TAS-120, reduced colony formation for wild-type FGFR2-IIIb-PPHLN1 but were ineffective against FGFR2-IIIb-N550K-PPHLN1 (Fig. 3B–C), indicating the resistance of the N550K mutation to TKIs. This suggests that the use of BGJ398 or TAS-120 against cancers driven by oncogenic FGFR2 proteins bearing the N550K mutation may be deleterious. The combination of the MEK inhibitor plus a TKI demonstrated a positive effect on colony reduction for both FGFR2-IIIb-PPHLN1 and FGFR2-IIIb-N550K-PPHLN1 (Fig. 3D,E). For cells expressing FGFR2-IIIb-N550K-PPHLN1, this was particularly significant given their resistance to treatment with either BGJ398 or TAS-120 alone (Fig. 3B,C). These results indicate the importance of determining the mutational status of the RTK in choosing effective treatment options.

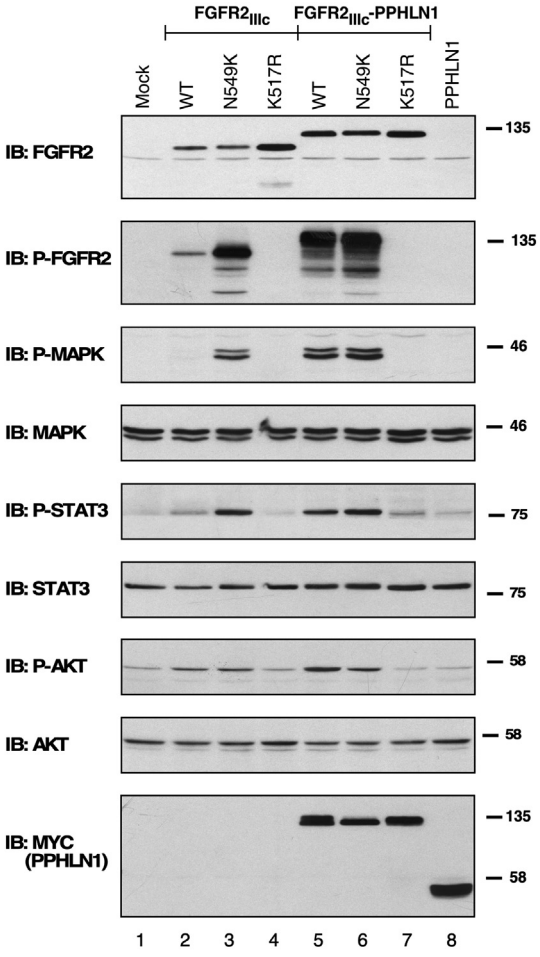

Fig. 2. Activation of downstream signaling pathways by FGFR2-PPHLN1. Lysates of HEK293T cells expressing either FGFR2-IIIc or FGFR2-IIIc-PPHLN1 derivatives were immunoblotted for total FGFR2 expression (1st panel). These lysates were also immunoblotted for phospho-FGFR (2nd panel), phospho-MAPK (T202, Y204) (3rd panel), phospho-STAT3 (Y705) (5th panel), and phospho-Akt (S473) (7th panel). Control immunoblots are shown for total expression of MAPK (4th panel), STAT3 (6th panel), and AKT (8th panel). Myc-tagged PPHLN1 proteins were detected by immunoblotting for Myc (9th panel). Shown are representative immunoblots of at least three independent experiments.

Effect of Trametinib and TKIs on FGFR2-PPHLN1 activation and downstream signaling

FGFR2-IIIc-PPHPLN1 proteins were expressed in HEK293T cells and lysates examined by immunoblotting. In cells expressing FGFR2-IIIc-PPHLN, treatment with Trametinib resulted in no significant difference in FGFR phosphorylation (Fig. 4A, lanes 1–4), as might be expected since Trametinib is a MEK inhibitor and not an FGFR inhibitor; however, a significant decrease in phospho-MAPK was observed at 5 nM, and complete inhibition at 50 nM. In cells expressing the kinase-activated FGFR2-IIIc-N549K-PPHLN1 (Fig. 4A, lanes 5–8), no inhibition of phospho-FGFR was observed in response to Trametinib; however, these cells showed only minimal inhibition of phospho-MAPK at 5 nM, although this signal was inhibited at 50 nM (Fig. 4A, lanes 5–8).

In response to TKI BGJ398, a reversible ATP-competitive TKI, cells expressing FGFR2-IIIc-PPHLN1 displayed a significant decrease in phospho-FGFR (Fig. 4B, lanes 1–4) at the higher concentrations of 30 nM and 100 nM. The inhibition of phospho-MAPK largely paralleled the inhibition of the phospho-FGFR signal. In marked contrast, cells expressing the kinase-activated FGFR2-IIIc-N549K-PPHLN1 (Fig. 4B, lanes 5–8), showed no inhibition of phospho-FGFR at any concentration of BGJ398, and only a partial inhibition of the phospho-MAPK signal at the two higher concentrations of 30 nM and 100 nM.

In response to TAS-120, an irreversible TKI, cells expressing FGFR2-IIIc-PPHLN1 displayed a significant decrease in phospho-FGFR (Fig. 4C, lanes 1–4) at all concentrations tested of 10 nM, 20 nM, and 50 nM. Again, the inhibition of phospho-MAPK largely paralleled the inhibition of the phospho-FGFR signal. In cells expressing the kinase-activated FGFR2-IIIc-N549K-PPHLN1 (Fig. 4C, lanes 5–8), some inhibition of phospho-FGFR was observed as the concentration of TAS-120 was increased to 10 nm, 20 nM, and 50 nM. These cells exhibited only a partial inhibition of phospho-MAPK at the two higher concentrations of TAS-120, 20 nM and 50 nM.

These results indicate that the MEK inhibitor Trametinib was generally effective in blocking downstream signaling in response to either FGFR2-IIIc-PPHLN1 or the activated mutant FGFR2-IIIc-N549K-PPHLN1. The TKIs BGJ398 and TAS-120, while effective in blocking FGFR activation and downstream MAPK signaling in response to FGFR2-IIIc-PPHLN1, showed little effect in inhibiting either FGFR activation or downstream MAPK signaling in response to the activated mutant.

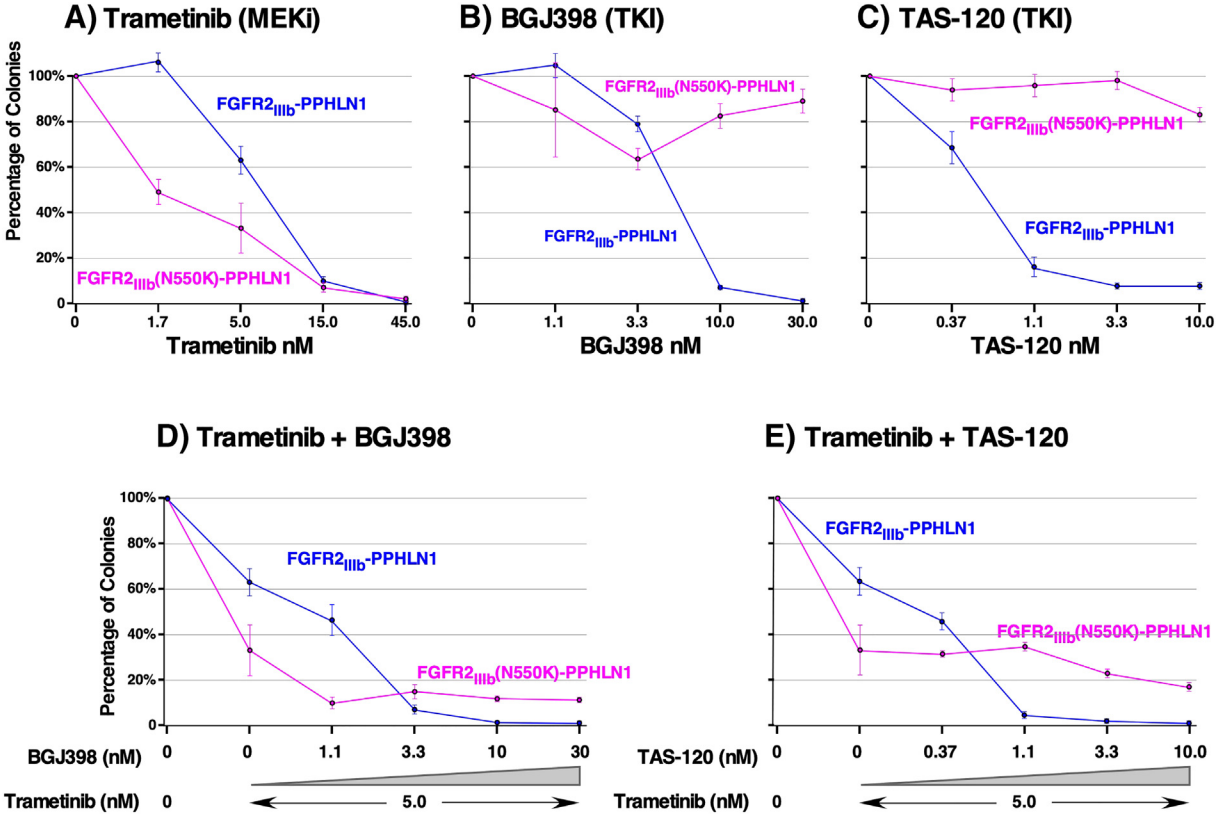

Fig. 3. Effects of TKIs and/or MEK inhibitor on biological activity of FGFR2-IIIb-PPHLN1 derivatives. RIE-1 cells stably expressing FGFR2-IIIb-PPHLN1 or FGFR2-III-N550K-PPHLN1 were plated in soft agar assays in the presence of: (A) Trametinib (0–45 nM), (B) BGJ398 (0–30 nM), (C) TAS-120 (0–10 nM), (D) Trametinib (0 and 5 nM) plus BGJ398 (0–30 nM) or (E) Trametinib (0 and 5 nM) plus TAS-120 (0–10 nM) for three weeks. These experiments were repeated a minimum of three times with triplicate plates for each inhibitor concentration, and were stained with crystal violet, photographed and quantitated. Samples with no inhibitor are set to 100%, ± SEM is shown. (For interpretation of the references to colour in this figure legend, the reader is referred to the web version of this article.)

To explore the synergistic effects of combining Trametinib with FGFR inhibition, cells were treated in combination with Trametinib and BGJ398 (Fig. 4D), or with Trametinib and TAS-120 (Fig. 4E). For cells expressing FGFR2-IIIc-PPHLN1 (Fig. 4D, lanes 1–5), a reduction in phospho-FGFR was not observed in the presence of Trametinib at lower concentrations of BGJ398, but at 15 nM BGJ398 a partial reduction was observed which was almost total at 50 nM. However, a significant reduction of phospho-MAPK was observed in these cells, similar to the reduction observed for Trametinib alone at 5 nM (Fig. 4A, lane 3). In cells expressing the kinase-activated FGFR2-IIIc-N549K-PPHLN1 in the presence of Trametinib plus BGJ398 (Fig. 4D, lanes 6–10), a partial reduction was observed for phospho-FGFR only at the highest concentration of 50 nM BGJ398. For these cells, in the presence of 5 nM Trametinib plus increasing concentrations of BGJ398, significant inhibition of the phospho-MAPK signal was observed at all concentrations.

With regard to Trametinib plus TAS-120 (Fig. 4E), for cells expressing FGFR2-IIIc-PPHLN1 (Fig. 4E, lanes 1–5), a reduction in phospho-FGFR was observed at all concentrations of TAS-120 tested. In cells expressing the kinase-activated FGFR2-IIIc-N549K-PPHLN1 in the presence of Trametinib plus TAS-120 (Fig. 4E, lanes 6–10), a partial reduction was observed for phospho-FGFR only at the highest concentration of 25 nM TAS-120 combined with Trametinib. For these cells, in the presence of 5 nM Trametinib plus increasing concentrations of TAS-120, although some inhibition of the phospho-MAPK signal was observed, this inhibition was only partial.

Membrane association is required for FGFR2-PPHLN1 activity

FGFR2-PPHLN1 preserves the transmembrane domain of FGFR2, which directs membrane insertion as a Type I transmembrane protein. The signal peptide of a Type I transmembrane protein is removed cotranslationally as the nascent protein enters the secretory pathway, where the extracellular domain also undergoes post-translational glycosylation [30,31].

Residues 2–26 were removed to create ΔSS-FGFR2-IIIc-PPHLN1 (Fig. 5A). Amino acid residues #2–26 at the N-terminus of the FGFR2 translation product represent the signal sequence, or signal peptide, which is at the N-terminus of the majority of newly synthesized proteins destined for the secretory pathway. This includes all RTKs, which are type I membrane-bound proteins; these are single-pass proteins which have their N-terminal domains targeted to the endoplasmic reticulum lumen during synthesis, and are anchored to the lipid membrane with a stop-transfer anchor sequence. Following cotranslational membrane insertion, modifications such as signal peptide cleavage, disulfide bond formation, and glycosylation occur during passage through the Golgi, after which the mature proteins reach the cell surface.

Separately, the extracellular and transmembrane domains of FGFR2-PPHLN1 were replaced with a short sequence encoding a myristylation signal, creating Myr–FGFR2–PPHLN1 (Fig. 5A). Myristylation conjugates myristic acid, a 14-carbon fatty acid, to the second residue Gly following removal of the N-terminal Met, thereby conferring membrane association without transmembrane insertion, nor does the resulting protein undergo glycosylation. Mutating this Gly residue to Ala (G2A) blocks the membrane-bound localization [17,18,32].

Using indirect immunofluorescence, FGFR2-IIIc-PPHLN1 was visualized at the plasma membrane, and also apparently localized in the ER/Golgi although this was not directly confirmed (Fig. 5Bi). Appendage of the myristylation signal resulted in plasma membrane localization (Fig. 5Biii). In contrast, ΔSS-FGFR2-IIIc-PPHLN1 was predominantly cytosolic (Fig. 5Bii), as was Myr*-FGFR2-PPHLN1 (Fig. 5Biv). The ΔSS proteins

were examined for glycosylation by digestion with Peptide:N-glycosidaseF (PNGaseF) (Fig. 5C). PNGaseF digestion of FGFR2 resulted in reduced electrophoretic mobility (Lanes 3–4), as was true for FGFR2-PPHLN1 (Lanes 7–8). In contrast, PNGaseF digestion of ΔSS-FGFR2-PPHLN1 (Lanes 5–6), or of ΔSS-FGFR2-IIIc (Lanes 9–10), resulted in no electrophoretic mobility shift. These results provide biochemical evidence of the altered localization of these proteins resulting from different localization signals.

Cell transformation assays showed that signal peptide deletion destroyed activity (Fig. 5D), which was restored by myristylation, but not by the mutant myristylation signal. These results indicate that FGFR2-PPHLN1 requires membrane association as an integral Type I transmembrane protein or by means of an N-terminal myristylation signal, and that the oncogenic activity of FGFR2-PPHLN1 is ligand-independent.

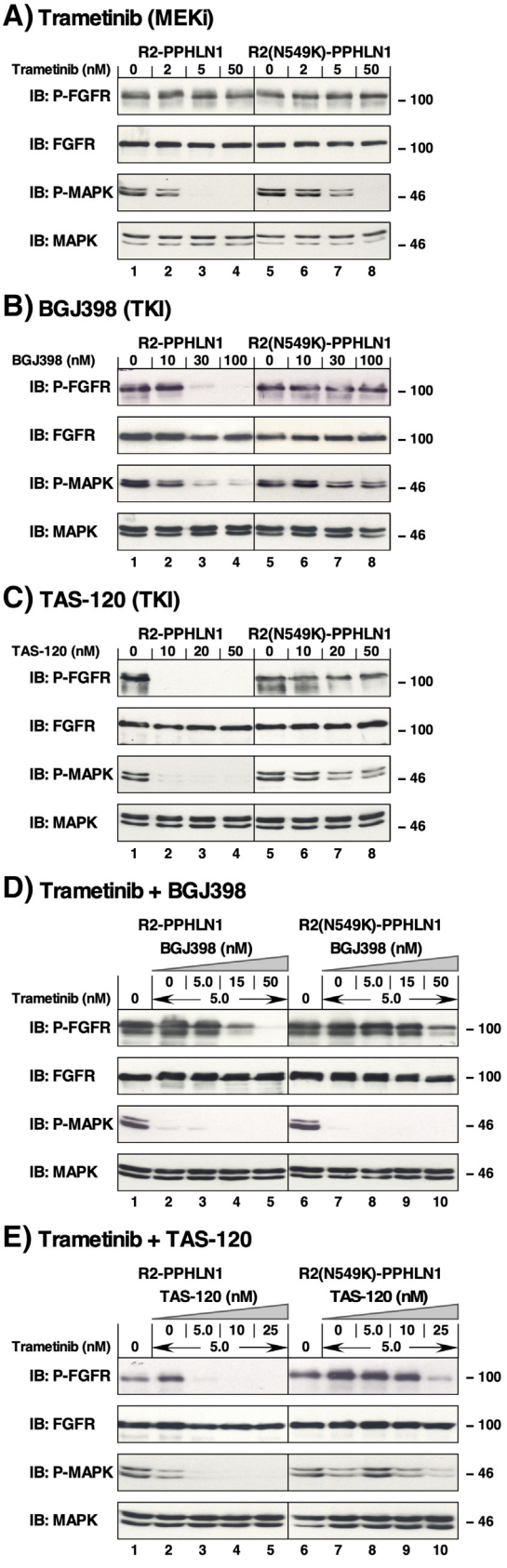

Discussion

The results presented here demonstrate that fusion of PPHLN1 at the C-terminus of FGFR2 confers constitutive activation to the receptor's tyrosine protein kinase. Constitutive activation of downstream signaling pathways was observed, including RAS/MAPK/ERK, JAK/STAT3 and PI3K/AKT (Fig. 2). Introduction of the kinase-dead mutation resulted in loss of FGFR2 kinase activity, and also blocked activation of downstream signaling pathways, indicating that FGFR2 kinase activity is obligatory for signaling by this fusion protein. The biological importance of this constitutive kinase activation was demonstrated by cell transformation assays; both FGFR2-IIIb-PPHLN1 and kinase-activated FGFR2-IIIb-N550K-PPHLN1 displayed abundant soft agar colony formation using epithelial RIE-1 cells and focus formation assay in NIH3T3 cells, shown in Fig. 1B and D with the quantitation shown in Fig. 1C and E.

Our results also indicate that FGFR2-IIIc-PPHLN1 must be localized to the plasma membrane in order to maintain its transforming ability. Removal of the N-terminal signal peptide blocked entrance into the secretory pathway and abolished activity (Fig. 5). Biological activity was restored by addition of a myristylation signal, facilitating association with the inner face of the plasma membrane (Fig. 5). This demonstrates that the transforming activity of FGFR2-PPHLN1 is completely ligand-independent, as the myristylated myr-FGFR2-PPHLN1 completely lacks the extracellular ligand binding domain. The requirement for membrane localization exhibited by FGFR2-PPHLN1 is similar to that demonstrated for another oncogenic fusion protein, FGFR3-TACC3 [17]; significantly, both fusion proteins have the FGFR-derived domain as their N-terminal moiety, which directs membrane localization and is required for biological activity. This observed phenotype could be attributed to access to essential downstream adaptor proteins such as FRS-2 that mediate FGFR signaling pathways. Not all oncogenic fusion proteins involving RTKs necessarily require membrane association, however, as evidenced by the apparently cytoplasmic/nuclear localization of BCR-ABL and BCR-FGFR1 [33,34]. Due to the localization requirement of FGFR2-PPHLN1, inhibition of membrane localization could serve as an alternative therapeutic strategy in targeting FGFR2-PPHLN1-driven ICC.

Collectively, we assessed differential sensitivities of FGFR2-PPHLN1 or FGFR2(N549/N550K)-PPHLN1 to different TKI treatments. Our data corroborate previous findings that ATP-competitive inhibitor BGJ398 alone

Fig. 4. Effects of TKIs and/or MEK inhibitor on signaling pathways of FGFR2-IIIc-PPHLN1 derivatives. (A) Lysates of HEK293T cells expressing FGFR2-IIIc-PPHLN1 and FGFR2-IIIc-N549K-PPHLN1 were treated with Trametinib (2 nM, 5 nM, or 50 nM) for 3 h. Lysates were immunoblotted for phospho-FGF receptor (Tyr653/654) (1st panel), overall FGFR2 expression (2nd panel), phospho-MAPK (T202/Y204) (3rd panel), and overall MAPK expression (4th panel). (B) Lysates of HEK293T cells expressing FGFR2-IIIc-PPHLN1 and FGFR2-IIIc-N549K-PPHLN1 were treated with BGJ398 (10 nM, 30 nM, or 100 nM) and immunoblotted as in (A). (C) Lysates of HEK293T cells expressing FGFR2-IIIc-PPHLN1 and FGFR2-IIIc-N549K-PPHLN1 were treated with TAS-120 (10 nM, 20 nM, or 50 nM) for 3 h. Lysates were analyzed as in (A). (D and E) Lysates of HEK293T cells expressing FGFR2-IIIc-PPHLN1 and FGFR2-IIIc-N549K-PPHLN1 were treated with either 5 nM of Trametinib in combination with 0 nM, 5 nM, 15 nM or 50 nM BGJ398 for 3 h, or with 5 nM of Trametinib in combination with 0 nM, 5 nM, 10 nM, or 25 nM TAS-120, and immunoblotted as in (A). Shown are representative immunoblots of at least three independent experiments.

may be ineffective to treat FGFR fusion proteins harboring kinase-activating mutations [35]. This result is consistent with previous studies showing that activating mutations in the FGFR kinase domain confer resistance to ATP-competitive inhibitors [9,13,33]. However, both FGFR2-PPHLN1 and FGFR2(N550K)-PPHLN1-expressing cells were sensitive to Trametinib. Furthermore, cells expressing FGFR2-IIIb-N550K-PPHLN1 remained sensitive to Trametinib, while combination treatment with either BJG398 or TAS-120 did not increase inhibition of phospho-MAPK. Although a significant synergistic effect was not observed with this combination treatment, it is critical to develop novel combination and targeted therapies as patients with FGFR2 gene fusion-driven ICC often develop activating mutations in the kinase domain, ultimately conferring resistance to TKI therapy [35]. Collectively, our results demonstrate the potential complexity of designing mutation-specific combinatorial treatment strategies for patients with FGFR2 activating mutation-positive malignancies. Lastly, the data presented here emphasize the need for additional targeted therapies to treat ICC.

Conclusions

With the advent of personalized medicine, the characterization of oncogenic fusion proteins arising from specific translocations such as t(10;12)(q26,q12) provides an opportunity to introduce molecular therapies. Our study demonstrates the potent biological activation and transforming potential of FGFR2-PPHLN1 in driving cellular proliferation in the genesis of ICC. Our data highlight the importance of sequencing-based, mutation-

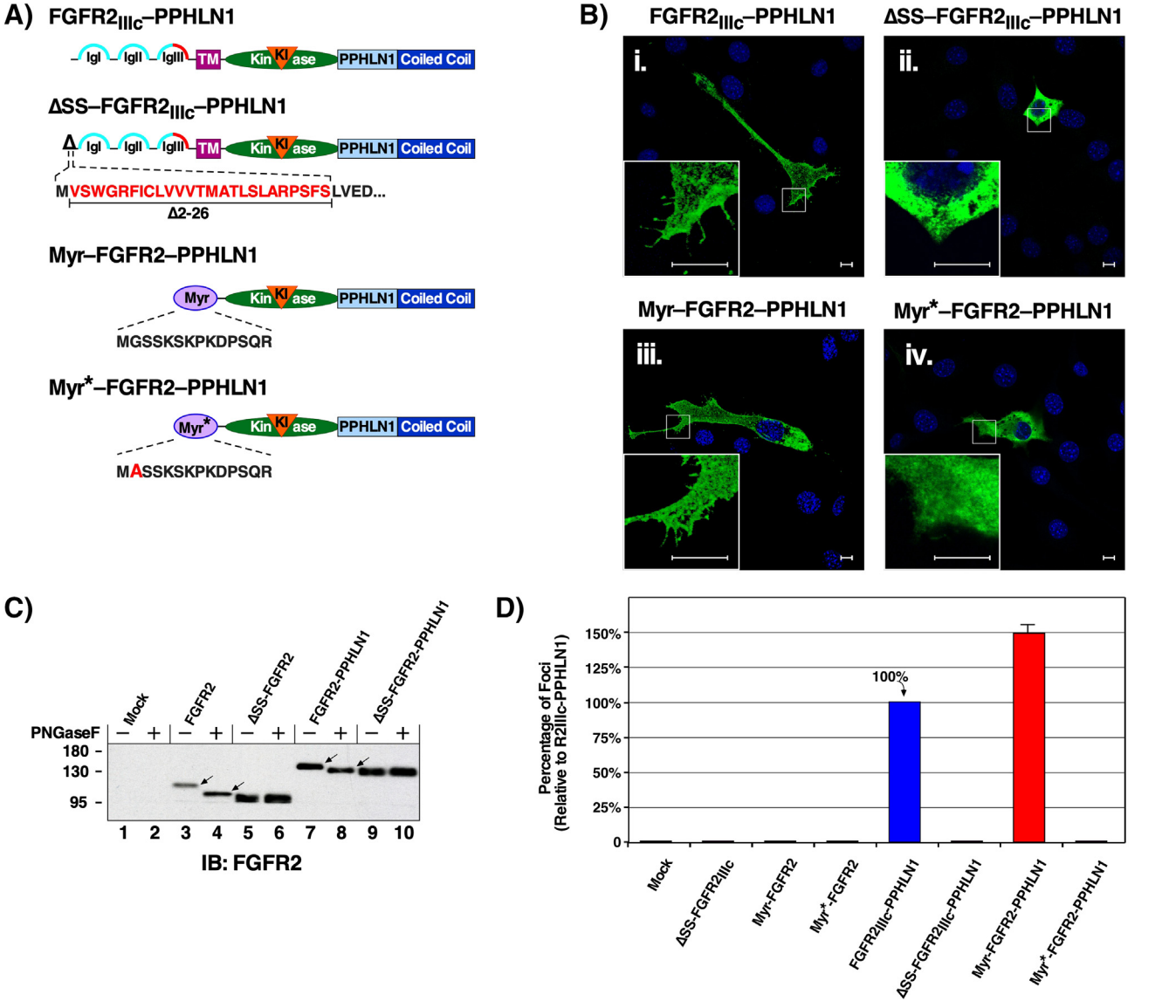

Fig. 5. FGFR2-PPHLN1 requires membrane association. (A) ΔSS-FGFR2IIIc-PPHLN1 indicates FGFR2IIIc-PPHLN1 with detail of signal sequence removed by deletion of amino acids #2–26. For the membrane-localized fusion construct, the extracellular and TM domains of FGFR2 were replaced with a myristylation sequence (Myr) derived from c-Src (Myr-FGFR2-PPHLN1). Mutation of Gly in position 2 in the myristylation signal to Ala (highlighted in red) abrogates myristylation, resulting in a Myr*-FGFR2-PPHLN1, which is not localized to the membrane. (B) Indirect immunofluorescence using a Leica SP8 inverted confocal microscope was used to visualize the subcellular localization of the indicated FGFR2-PPHLN1 proteins expressed in NIH3T3 cells, using a primary antiserum to detect the myc-tagged PPHLN1 domain in each fusion protein. Note clear delineation of plasma membrane in (i) and (iii). Areas highlighted in inserts are enlarged 5×. Length bars = 10 μm. (C) HEK293T cell lysates expressing indicated proteins were treated ± PNGaseF enzyme to remove N-linked oligosaccharides and immunoblotted with FGFR2 antibody. Removal of N-linked oligosaccharide is clearly indicated by altered electrophoretic mobility, observed for native FGFR2 (Lane 4 vs Lane 3), and for FGFR2-PPHLN1 (Lane 8 vs Lane 7). (D) Transformation of NIH3T3 cells by FGFR2 and FGFR2-IIIc-PPHLN1 derivatives. Number of foci were scored, normalized by transfection efficiency, and quantitated relative to FGFR2-IIIc-PPHLN1 ± SEM. Assays were performed a minimum of three times per DNA construct. (For interpretation of the references to colour in this figure legend, the reader is referred to the web version of this article.)

specific personalized therapeutics in treating FGFR2 fusion-positive ICC patients.

Author contributions

F.L. contributed to Conceptualization, Methodology, Validation, Investigation, Data Curation, Writing - Original Draft, Writing - Review & Editing; A.N.M. contributed to Conceptualization, Methodology, Validation, Investigation, Data Curation, Writing - Original Draft, Writing - Review & Editing, Supervision; N.M.P. contributed to Conceptualization, Methodology, Validation, Investigation, Data Curation, Writing - Original Draft, Writing - Review & Editing; K.N.N. contributed to Conceptualization, Methodology, Validation, Investigation; and D.J.D. contributed to Conceptualization, Methodology, Validation, Investigation, Data Curation, Writing - Original Draft, Writing - Review & Editing, Visualization, Supervision, Project administration.

Declaration of competing interest

The authors declare that they have no known competing financial interests or personal relationships that could have appeared to influence the work reported in this paper.

Acknowledgements

We thank Dr. Lars Eckmann (UC San Diego) for generously providing RIE-1 cells. We thank all current lab members particularly Juyeon Ko, Clark Wang, and Dalida Warda for encouragement and critical reading of the manuscript. This work was supported by a UC San Diego San Diego Fellowship (to M.N.P), and a grant from the UC San Diego Foundation (to D.J.D.)

References

[1] A. Moeini, D. Sia, N. Bardeesy, V. Mazzaferro, J.M. Llovet, Molecular pathogenesis and targeted therapies for intrahepatic cholangiocarcinoma, Clin. Cancer Res. 22 (2016) 291–300.
[2] D. Sia, V. Tovar, A. Moeini, J.M. Llovet, Intrahepatic cholangiocarcinoma: Pathogenesis and rationale for molecular therapies, Oncogene. 32 (2013) 4861–4870.
[3] M.J. Borad, M.D. Champion, J.B. Egan, W.S. Liang, R. Fonseca, A.H. Bryce, et al., Integrated genomic characterization reveals novel, therapeutically relevant drug targets in FGFR and EGFR pathways in sporadic intrahepatic cholangiocarcinoma, PLoS Genet. 10 (2014), e1004135.
[4] Y. Arai, Y. Totoki, F. Hosoda, T. Shirota, N. Hama, H. Nakamura, et al., Fibroblast growth factor receptor 2 tyrosine kinase fusions define a unique molecular subtype of cholangiocarcinoma, Hepatology. 59 (2014) 1427–1434.
[5] D. Sia, B. Losic, A. Moeini, L. Cabellos, K. Hao, K. Revill, et al., Massive parallel sequencing uncovers actionable FGFR2-PPHLN1 fusion and ARAF mutations in intrahepatic cholangiocarcinoma, Nat. Commun. 6 (2015) 6087.
[6] L.H. Gallo, K.N. Nelson, A.N. Meyer, D.J. Donoghue, Functions of fibroblast growth factor receptors in cancer defined by novel translocations and mutations, Cytokine Growth Factor Rev. 26 (2015) 425–449.
[7] M.K. Webster, D.J. Donoghue, FGFR activation in skeletal disorders: too much of a good thing, Trends Genet. 13 (1997) 178–182.
[8] S. Kazerounian, S. Aho, Characterization of periphilin, a widespread, highly insoluble nuclear protein and potential constituent of the keratinocyte cornified envelope, J. Biol. Chem. 278 (2003) 36707–36717.
[9] F. Li, M.N. Peiris, D.J. Donoghue, Functions of FGFR2 corrupted by translocations in intrahepatic cholangiocarcinoma, Cytokine Growth Factor Rev. 52 (2020) 56–67.
[10] M. Javle, M. Lowery, R.T. Shroff, K.H. Weiss, C. Springfeld, M.J. Borad, et al., Phase II study of BGJ398 in patients with FGFR-altered advanced cholangiocarcinoma, J. Clin. Oncol. 36 (2018) 276–282.
[11] J.W. Valle, A. Lamarca, L. Goyal, J. Barriuso, A.X. Zhu, New horizons for precision medicine in biliary tract cancers, Cancer discovery. 7 (2017) 943–962.
[12] L. Goyal, S.K. Saha, L.Y. Liu, G. Siravegna, I. Leshchiner, L.G. Ahronian, et al., Polyclonal secondary FGFR2 mutations drive acquired resistance to FGFR inhibition in patients with FGFR2 fusion-positive cholangiocarcinoma, Cancer discovery. 7 (2017) 252–263.
[13] S.A. Byron, H. Chen, A. Wortmann, D. Loch, M.G. Gartside, F. Dehkhoda, et al., The N550K/H mutations in FGFR2 confer differential resistance to PD173074, dovitinib, and ponatinib ATP-competitive inhibitors, Neoplasia. 15 (2013) 975–988.
[14] L. Goyal, L. Shi, L.Y. Liu, F. Fece de la Cruz, J.K. Lennerz, S. Raghavan, et al., TAS-120 overcomes resistance to ATP-competitive FGFR inhibitors in patients with FGFR2 fusion-positive intrahepatic cholangiocarcinoma, Cancer discovery. 9 (2019) 1064–1079.
[15] S.C. Robertson, A.N. Meyer, K.C. Hart, B.D. Galvin, M.K. Webster, D.J. Donoghue, Activating mutations in the extracellular domain of the fibroblast growth factor receptor 2 function by disruption of the disulfide bond in the third immunoglobulin-like domain, Proc. Natl. Acad. Sci. U. S. A. 95 (1998) 4567–4572.
[16] B.D. Galvin, K.C. Hart, A.N. Meyer, M.K. Webster, D.J. Donoghue, Constitutive receptor activation by Crouzon syndrome mutations in fibroblast growth factor receptor (FGFR)2 and FGFR2/Neu chimeras, Proc. Natl. Acad. Sci. U. S. A. 93 (1996) 7894–7899.
[17] K.N. Nelson, A.N. Meyer, C.G. Wang, D.J. Donoghue, Oncogenic driver FGFR3-TACC3 is dependent on membrane trafficking and ERK signaling, Oncotarget. 9 (2018) 34306–34319.
[18] M.K. Webster, D.J. Donoghue, Enhanced signaling and morphological transformation by a membrane-localized derivative of the fibroblast growth factor receptor 3 kinase domain, Mol. Cell. Biol. 17 (1997) 5739–5747.
[19] H. Liu, J.H. Naismith, An efficient one-step site-directed deletion, insertion, single and multiple-site plasmid mutagenesis protocol, BMC Biotechnol. 8 (2008) 91.
[20] A.D. Miller, G.J. Rosman, Improved retroviral vectors for gene transfer and expression, Biotechniques 7 (1989) 980–982 (4-6, 9-90).
[21] L.H. Gallo, A.N. Meyer, K. Motamedchaboki, K.N. Nelson, M. Haas, D.J. Donoghue, Novel Lys63-linked ubiquitination of IKKbeta induces STAT3 signaling, Cell Cycle 13 (2014) 3964–3976.
[22] C.A. Bell, J.A. Tynan, K.C. Hart, A.N. Meyer, S.C. Robertson, D.J. Donoghue, Rotational coupling of the transmembrane and kinase domains of the Neu receptor tyrosine kinase, Mol. Biol. Cell 11 (2000) 3589–3599.
[23] A.N. Meyer, C.W. McAndrew, D.J. Donoghue, Nordihydroguaiaretic acid inhibits an activated fibroblast growth factor receptor 3 mutant and blocks downstream signaling in multiple myeloma cells, Cancer Res. 68 (2008) 7362–7370.
[24] K.N. Nelson, A.N. Meyer, A. Siari, A.R. Campos, K. Motamedchaboki, D.J. Donoghue, Oncogenic gene fusion FGFR3-TACC3 is regulated by tyrosine phosphorylation, Mol. Cancer Res. 14 (2016) 458–469.
[25] G.A. Bellus, I. McIntosh, E.A. Smith, A.S. Aylsworth, I. Kaitila, W.A. Horton, et al., A recurrent mutation in the tyrosine kinase domain of fibroblast growth factor receptor 3 causes hypochondroplasia, Nat. Genet. 10 (1995) 357–359.
[26] M.G. Gartside, H. Chen, O.A. Ibrahimi, S.A. Byron, A.V. Curtis, C.L. Wellens, et al., Loss-of-function fibroblast growth factor receptor-2 mutations in melanoma, Mol. Cancer Res. 7 (2009) 41–54.
[27] L. Dailey, D. Ambrosetti, A. Mansukhani, C. Basilico, Mechanisms underlying differential responses to FGF signaling, Cytokine Growth Factor Rev. 16 (2005) 233–247.
[28] V.P. Eswarakumar, I. Lax, J. Schlessinger, Cellular signaling by fibroblast growth factor receptors, Cytokine Growth Factor Rev. 16 (2005) 139–149.
[29] J.Y. Cha, Q.T. Lambert, G.W. Reuther, C.J. Der, Involvement of fibroblast growth factor receptor 2 isoform switching in mammary oncogenesis, Mol. Cancer Res. 6 (2008) 435–445.
[30] J. Tanizaki, D. Ercan, M. Capelletti, M. Dodge, C. Xu, M. Bahcall, et al., Identification of oncogenic and drug-sensitizing mutations in the extracellular domain of FGFR2, Cancer Res. 75 (2015) 3139–3146.
[31] L. Duchesne, B. Tissot, T.R. Rudd, A. Dell, D.G. Fernig, N-glycosylation of fibroblast growth factor receptor 1 regulates ligand and heparan sulfate co-receptor binding, J. Biol. Chem. 281 (2006) 27178–27189.
[32] M.P. Kamps, J.E. Buss, B.M. Sefton, Mutation of NH2-terminal glycine of p60src prevents both myristoylation and morphological transformation, Proc. Natl. Acad. Sci. U. S. A. 82 (1985) 4625–4628.
[33] M.N. Peiris, F. Li, D.J. Donoghue, BCR: a promiscuous fusion partner in hematopoietic disorders, Oncotarget. 10 (2019) 2738–2754.
[34] M.N. Peiris, A.N. Meyer, K.N. Nelson, E.W. Bisom-Rapp, D.J. Donoghue, Oncogenic fusion protein BCR-FGFR1 requires BCR-mediated oligomerization and chaperonin Hsp90 for activation, Haematologica. 105 (2020) 1262–1273.
[35] S. Rizvi, G.J. Gores, Fibroblast growth factor receptor inhibition for cholangiocarcinoma: looking through a door half-opened, Hepatology. 68 (2018) 2428–2430.